Identifying potential off-target protein binders of Glutamate-Ureido-Lysine**, a prostate cancer specific imaging agent**

Martin K. Bakht[1,2,3,4,5¶], John J. Hayward[1¶], Farsheed Shahbazi-Raz[1¶], Daniel Meister[1], Adam Pillon[2], Mathew Stover[2], Adam Tronchin[2], Lavleen Mader[1], Bre-Anne Fifield[2], Sheng-Yu Ku[4,5], Gi Jeong Cheon[3], Keon Wook Kang[3], Yuzhuo Wang[6], Xuesen Dong[6], Himisha Beltran[4,5], Lisa A. Porter[2*], John F. Trant[1*]

[1]*Department of Chemistry and Biochemistry, University of Windsor, Windsor, Ontario, Canada*

[2]*Department of Biomedical Sciences, University of Windsor, Windsor, Ontario, Canada*

[3]*Department of Nuclear Medicine, Seoul National University College of Medicine, Seoul, Korea*

[4]*Dana Farber Cancer Institute and Harvard Medical School, Boston, Massachusetts, USA*

[5]*Broad Institute of Harvard and MIT, Cambridge, Massachusetts, USA*

[6]*Vancouver Prostate Centre, University of British Columbia, Vancouver, British Columbia, Canada*

[¶] These authors contributed equally to this work.

Co-corresponding authors*:

***Lisa A. Porter,** PhD*

lporter@uwindsor.ca

***John F. Trant,** PhD*

J.Trant@uwindsor.ca

ABSTRACT

Prostate-specific membrane antigen (PSMA) is highly overexpressed in most prostate cancers and is clinically visualized using PSMA-specific probes incorporating Glutamate-Ureido-Lysine (GUL). PSMA is effectively absent from certain high-mortality, treatment-resistant subsets of prostate cancers, such as neuroendocrine prostate cancer (NEPC); however, GUL-based probes still sometimes identify NEPC metastatic tumours. These probes may bind unknown proteins associated with PSMA-suppressed cancers. We identified the upregulation of PSMA-like aminopeptidase NAALADaseL and the metabotropic glutamate receptors (mGluRs) in NEPC; we found that the expression levels inversely correlate with PSMA expression and are associated with poor clinical prognosis indicating they may participate in NEPC disease progression. Computationally predicting that GUL-based probes bind well to these targets, we designed and synthesized a new fluorescent probe to investigate these proteins *in vitro*, where it shows excellent affinity for PSMA, NAALADaseL and specific mGluRs associated with poor prognosis.

Key words: PSMA, prostate cancer, Glutamate-Ureido-Lysine, molecular imaging, PET, glutamate receptors, neuroendocrine

Introduction

In 2020, 190,000 American men will be diagnosed with, and 33,300 will die from, prostate cancer. Although mortality has fallen 52% from its 1993 peak, prostate cancer remains a leading cause of cancer death.[2] The use of positron emission tomography (PET) imaging for accurate diagnosis and localization of tumours has started to improve prostate cancer staging, improving patient management.[3] Prostate-specific membrane antigen (PSMA), a cell surface

protein expressed in the majority of prostate cancers, can be visualized by PET imaging employing radiolabeled antibodies. Next-generation imaging agents based on small molecule moieties, particularly the PSMA-targeting peptidomimetic Glutamate-Ureido-Lysine (GUL), demonstrate superior pharmacokinetics (fast tumor uptake, and rapid blood clearance) over the radiolabeled PSMA antibodies (**Fig. 1a**).[4] GUL's molecular mode of action however, is not completely understood.[5, 6] The leading clinical candidates are ^{68}Ga-labeled PSMA-11 (**Ga-GUL**),[7] where the GUL core is conjugated to an acyclic hexadentate gallium ligand; and ^{18}F-PSMA-1007 (**F-GUL**)[8] where GUL is connected to a *pseudo*peptide functionalized with an ^{18}F isotope (**Fig. 1a**).[9, 10]

PSMA, a type II glutamate carboxypeptidase encoded by the folate hydrolase 1 gene (*FOLH1*),[11, 12] is expressed primarily in the duodenum, small intestine, nervous system, salivary gland and prostate.[13] It modulates glutamate signaling induced by the metabotropic glutamate receptor (mGluR) pathway,[14] cleaving glutamate from both dietary folic acid and the neurotransmitter *N*-acetyl-L-aspartyl-L-glutamate (NAAG). PSMA overexpression is a hallmark of prostate cancer including metastatic castration resistant prostate adenocarcinoma.[15, 16] Despite this, both immunohistochemical and genomic data have demonstrated that PSMA is expressed at only very low levels, if at all, in neuroendocrine prostate cancer (NEPC),[17] an aggressive form of androgen-receptor (AR)-independent prostate cancer with exceedingly high mortality rates.[17, 18]

While *de novo* NEPC is rare, this hard-to-treat phenotype can emerge as a prostate cancer resistance mechanism to AR-targeted therapies, shedding the PSMA biomarker concurrent with a downregulation of the AR.[18, 19, 20] As GUL-PET modalities target PSMA, they are not expected to be effective for diagnosing NEPC. A less specific agent, ^{18}F-fluorodeoxyglucose, which exploits cancer cells' increased glucose-uptake, is often used for NEPC imaging similar to small cell lung cancer.[21, 22] Unexpectedly, a recent study
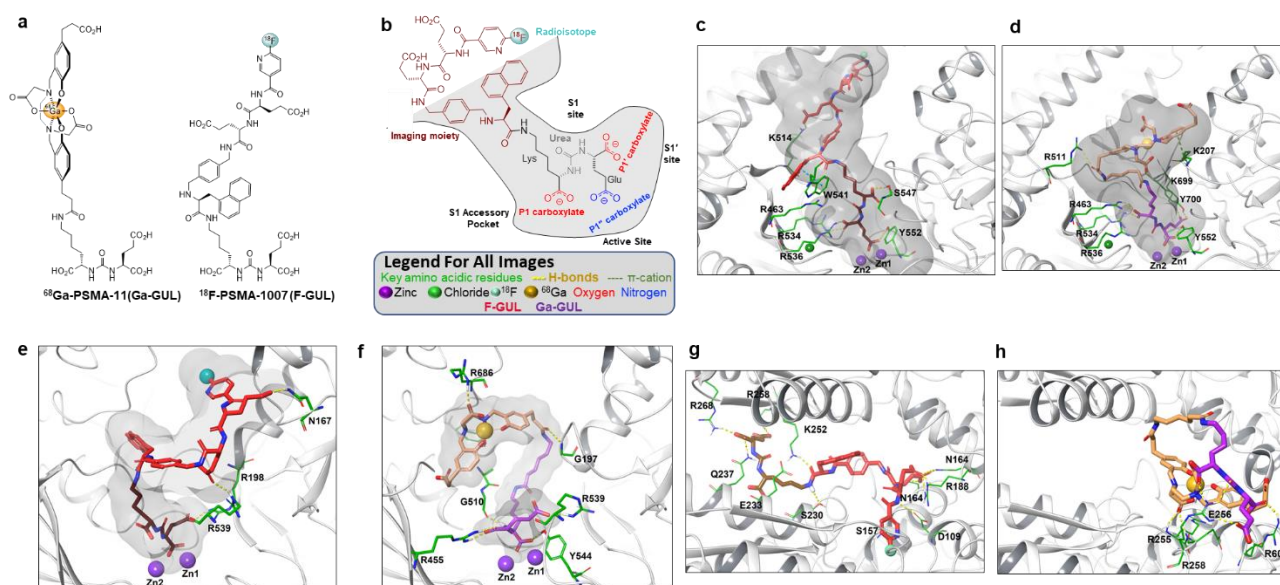
Fig. 1 Structure of clinical PSMA probes and their binding modes within the PSMA, NAALADaseL and mGlur8 active sites. (**a**) Structure of **Ga-GUL** and **F-GUL**. (**b**) **F-GUL** within the PSMA active site, showing the different regions of the active site and the substructure nomenclature of the probe. Computational modelling of (**c**) **F-GUL** and (**d**) **Ga-GUL** within the PSMA active site (*2XEG*), (**e**) **F-GUL** and (**f**) **Ga-GUL** within the NAALADaseL active site (*4TWE*) and (**g**) **F-GUL** and (**h**) **Ga-GUL** within the mGlur8 active site (*6BSZ*). The imaging moieties are shown in red (**F-GUL**) and beige (**Ga-GUL**) with the GUL moiety in brown (**F-GUL**) and purple (**Ga-GUL**). Key residues which form strong interactions—H-bonds (yellow dashed lines), π-cation (green dashed line)—are highlighted in green; and zinc, chlorine, gallium and fluorine atoms are spheres coloured purple, green, blue and orange respectively.

demonstrated that GUL-based imaging can detect NEPC tumours despite the tumour's apparent PSMA-negativity.[23] This is important, as PSMA-levels can vary significantly even within a single patient.[24] Furthermore, although PSMA expression is correlated with GUL-radioligand uptake,[25] the correlation is not perfect and tumours with low PSMA expression may also be detected using GUL-based probes.[23] GUL-based probes have also resulted in false positive interpretations among patients with a history of radiotherapy.[26] Together, the evidence suggests that GUL interacts fortuitously with other prostate cancer-associated proteins. Identifying these targets, and determining whether they are indicative of NEPC, is a pressing clinical goal.

The mGluRs and the aminopeptidase NAALADaseL1 are both PSMA-related type II transmembrane peptidases involved in glutamate signaling. We hypothesized that these

4

proteins might be responsible for GUL's off-target positive results in NEPC. In this study, we investigated this question with a cross-disciplinary combination of computational chemistry, synthesis and histochemical application of a new fluorescent probe, mining of clinical data, *in vitro* over-expression of the suspected proteins, and *in vivo* patient-derived xenograft (PDX) models.

F-GUL and Ga-GUL are predicted to have high affinity for PSMA. GUL-based probes interact with three components of PSMA's active site: the zinc ions, the pharmacophore (S1′) pocket, and the hydrophobic S1 accessory pocket (**Fig. 1b**).[27] PSMA's active site hosts two Zn^{2+} ions, responsible for substrate cleavage (**Fig. S1**Error! Reference source not found.**a**).[28, 29] The S1′ site, highly specific for glutamate, determines substrate specificity.[30] The large hydrophobic S1 accessory pocket, hosting the rest of the substrate, is far more promiscuous allowing for binding of both folate and NAAG.[31]

To better understand probe-protein interactions, *in silico* docking studies were performed between the two GUL radiolabels and a computationally-relaxed PSMA protein (PDB: *2XEG*).[32] Although the ligands' conformations differ (**Fig. 1c-d**), both share similar interactions with the same Tyr552 active site residue and the Zn atoms (**Fig. S1b**) but **F-GUL** does not extend into the S1′ site like **Ga-GUL** does. Both probes are predicted to have high affinity for PSMA, with induced fit docking scores around −15 kcal/mol (Table 1). Computed binding modes are consistent with the previously hypothesized interactions.[30, 33, 34]

The P1″ glutamate carboxylate moiety of **F-GUL** (**Fig. 1c**) forms strong interactions with the zincs (2.06 Å and 1.95 Å), and a strong hydrogen bond (2.06 Å) to the phenolic H of the S1′ Tyr552. A major structural feature of PSMA's S1 site is the "accessory pocket," whose entrance lid comprises three arginine residues (Arg536, Arg534, and Arg463) that can flip open to accommodate larger molecules. The P1′ carboxylate of **F-GUL** is stabilized by H-bonds with these residues Arg536 (1.73 Å) and Arg534 (1.67 Å); while the P1 carboxylate has a

strong H-bond interaction with nearby Ser547. The rigidity of the **F-GUL** linker enables the radiolabel-bearing moiety to remain inside the pocket. This results in a likely important π-π interaction with Trp541 and several H-bonds with Lys514 (**Fig S2a**).

Ga-GUL's longer nine-atom linker enables it to enter deeper, properly occupying the S1′ pocket (**Fig. 1d**), engaging in H-bonds with Lys699 (1.81 Å) and Tyr700 (1.85 Å) through the P1″ acid, and Tyr552 (1.70 Å) through the P1′ acid. The P1 glutamate carboxylate forms an isosceles triangle interaction with 2.18 Å distances to both zinc ions. Ga-GUL's long linker forms H-bonds with Arg511 and a key π-cation interaction with Lys207 that guides the probe into place (**Fig S2b**).

This structural tour, consistent with the literature,[35] gave us confidence in the binding mode of the probes. Consequently, we extended this approach to the two NEPC-suspect proteins.

F-GUL and Ga-GUL bind NAALADaseL1 and mGluR8. F-GUL's GUL moiety **Suppl. Video 2**binds to NAALADaseL1 in a manner reminiscent of **Ga-GUL**'s PSMA binding, occupying the S1′ pocket due to NAALADaseL1's larger, more open pocket (**Fig. 1e**). **F-GUL**'s P1″ glutamate carboxylate forms an H-bond with Arg198, while the P1′ carboxylate bridges $Zn(1)^{2+}$ and $Zn(2)^{2+}$ at distances of 2.07 Å and 2.27 Å, respectively. **F-GUL**'s aromatic domains are positioned on the outer surface of the receptor, stabilized by a series of H-bond interactions with Asn167 and Arg539 (**Fig. S2d**). The carboxylates of **Ga-GUL**'s glutamates adopt analogous positions (**Fig. 1f**), but the linker takes a very different path out of the active site through the wide channel (**Fig. S1c**); Arg539–P1″ carboxylate, Arg455–P1′ carboxylate and Gly510–ureido carbonyl H-bonds hold the linker in conformation. The **Ga-GUL** P1′ carboxylate interacts with $Zn(1)^{2+}$ and $Zn(2)^{2+}$ at distances of 2.17 Å and 2.09 Å, respectively (**Fig. S2e**). The subtly different structure clearly induces differences in conformation (**Fig.**

S1c), but docking scores predict both ligands to be excellent partners for the accommodating NAALADaseL1 (**Table 1**).

Table 1 Docking scores for the probes with the target proteins from both rigid and induced docking models (kcal/mol).

Receptor	Ligand	Docking Score (kcal/mol)	
		RRD Score	IFD Score
PSMA	Cy3-GUL	−12.93	−13.73
	Ga-GUL	−11.29	−13.10
	F-GUL	−11.66	−14.83
NAALADaseL	Cy3-GUL	−9.09	−10.83
	Ga-GUL	−1.69	−12.25
	F-GUL	−8.20	−12.91
mGluR8	Cy3-GUL	−8.15	−11.28
	Ga-GUL	−4.09	−6.64
	F-GUL	−7.67	−13.16

The mGluRs always self-assemble into homodimers *in vivo*. The probes were docked (without restrictions) to each of the eight mGluR homodimers, but showed the best affinity for mGluR1, mGluR5 and mGluR8 (**Table S3**). Curiously, the probes do not interact with the glutamate-binding active site of these proteins, which is far narrower than either PSMA's or NAALADaseL1's; instead, they bind to the large inter-monomer cleft (**Fig. 1g-h**). Induced-fit docking predicts the best binding to mGluR5 and 8, with scores on par with NAALADaseL1 and only slightly inferior to PSMA (**Tables 1** and **S3**). The docking scores to the other mGluRs were lower (−5.2 to −13.2) but remain favourable. Molecular dynamics simulations helped us understand the high docking score and the unusual binding mode of the probes with mGluR8, which we identified as being particularly NEPC relevant (*vide infra*). Very little movement is observed within the binding cleft for either ligand: most structures fall within a 1 Å cluster (**Fig**

S4Error! Reference source not found.) due to an extensive hydrogen bonding network that forms between the positively charged residues of the cleft and the negatively charged probes (**Fig. S5-S16**). However, the two probes bind very differently despite both having strong affinity (**Fig S1d**), possible due to the large size of the cleft. **F-GUL** (**Fig. 1g**) is particularly stable, adopting an extended conformation maximizing hydrogen bonding interactions between the glutamate and the highly positive interprotein region's residues Arg188, Arg240 of one monomer, and Ser157, Asn226, Lys252, Arg255, and Arg268 in the other (**Fig. S2g**). **Ga-GUL** (**Fig. 1h**) forms far fewer interactions and instead folds in on itself, held together by an intramolecular hydrogen bond; but it still interacts with Ser200, Gln237, Asn186, of one monomer and Arg60 and Arg255 in the other. Both complexes are highly stabilized through these interactions making mGluR8 an exceptional potential molecular target (**Fig. S2h**).

These data predict that both **F-GUL** and **Ga-GUL** will have strong affinity, comparable to PSMA, for both NAALADaseL1 and a subset of mGluRs. It is conceivable that these two protein classes are responsible for the GUL probes' efficacy in detecting PSMA-suppressed cancers; however, it is unknown whether these proteins are associated with NEPC.

Aminopeptidase NAALADaseL1 is elevated in NEPC. NAALADaseL1, encoded by *NAALADL1*, has high sequence similarity to PSMA (**Fig. S3**).[36] They share more than 90% structurally equivalent residues, with near complete identity at the active site (**Fig. S3**, PDB: *2XEJ* and *4TWE*).[37] We examined the expression of NAALADaseL1 using the LTL331 patient-derived xenograft model of prostate cancer progression from adenocarcinoma-to-NEPC (**Fig. 2a**).[38] *NAALADL1* gene expression
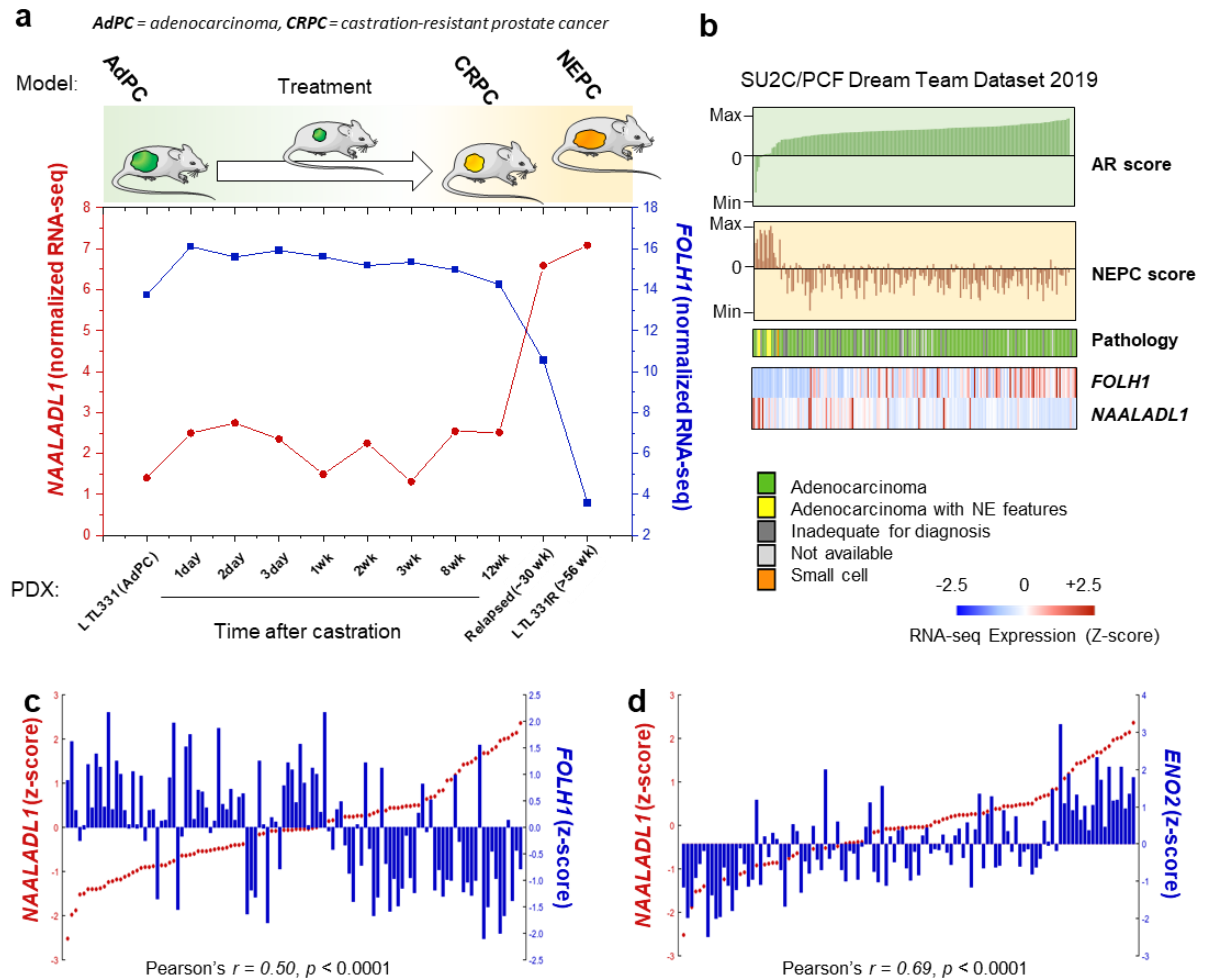
Fig. 2 Differential expression of NAALADL1 in NEPC as an alternative target for GUL-ligands. (a) Schematic of our established PDX mice models of adenocarcinoma (AdPC) and NEPC, and alteration of *FOLH1* and *NAALADL1* gene expression during the transition from AdPC to NEPC; **(b)** Evaluation of the expression of FOLH1 and *NAALADL1* genes and their association with AR and NEPC scores in the SU2C/PCF Dream Team Dataset 2019.[1] The high levels of *NAALADL1* gene expression in AdPC is associated with both lower levels of *FOLH1* gene expression and higher levels of *ENO2* gene expression, the archetypal NE-marker; **(c)** Pearson's correlation between *FOLH1* (blue) and *NAALADL1* (red) expression levels; **(d)** Pearson's correlation between *ENO2* (blue) and *NAALADL1* (red) expression levels among AdPC samples (n = 199) generated by R2: Genomics Analysis and Visualization Platform (http://r2.amc.nl).

remains minimal during the effective treatment period, but spikes as the tumour becomes resistant to therapy and peak expression occurs when the tumour transitions to NEPC. This profile inversely correlates with that of *FOLH1* (**Fig. 2a**). This trend is mirrored in the Dream Team patient dataset (**Fig. 2b**);[1] when ordering patients by increasing AR expression, *NAALADL1* expression falls while PSMA expression increases; furthermore, NEPC score is

strongly positively correlated with *NAALADL1* expression. As NAALADaseL1 is elevated in low-PSMA prostate cancers with an NEPC gene signature (**Fig. 2c-d**), this data supports the computational supposition that NAALADaseL1 may be one target of the GUL probes on PSMA-suppressed cells.

mGluRs are upregulated during progression to NEPC. The second class of proteins identified for investigation were the mGluRs. While increased expression of mGluR2 has already been reported in PSMA-positive cancers,[14] we observed a significant upregulation in the expression of most mGluR family members during cancer progression from normal prostate adenocarcinoma (HSPC) to NEPC in our PDX mouse model (**Fig. 3a-b**). Following castration, *GRM 2, 3, 4* and *8* all become increasingly expressed as *FOLH1* downregulates. Furthermore, their expression is strongly positively correlated to that of *SRRM4*, which is the archetypal biomarker of NEPC (**Fig. S17**). Data mining the Memorial Sloan Kettering Cancer Center cohort[39] for prostate tumor survival, identifies that high levels of *GRM1, 3, 4,* and especially *5* and *8* are correlated with shorter times to biochemical recurrence, with *GRM8* showing the most significant effect (**Fig. S18**). Further investigation revealed that *GRM8* expression is low in both benign tumours and in localized hormone sensitive prostate cancer (HSPC), but it rises markedly in metastatic disease (**Fig. S19)**. Our analysis shows that its expression rises during the transition to castration-resistant prostate cancer and can be significantly elevated in histopathologically-confirmed NEPC (**Fig. 3c**). The mGluRs are clearly associated with NEPC, and their molecular role deserves further attention and investigation. Together with NAALAD1, the biochemical and computational data all suggest that the GUL probes might have two proteins that can explain their binding to PSMA-suppressed cells.

A novel synthetic fluorescent Cy3-GUL probe is predicted to bind to all three proteins. To validate this hypothesis, we analyzed our predicted binding modes of **F-GUL** and **Ga-GUL** to design a novel cyanine dye-incorporating fluorescent probe (**Cy3-GUL**, **Fig. 3d**) analogue

of the clinical radiolabels (**Fig. 4**). A series of related probes with different linkers were computationally screened using docking, but the best binding results were observed for a synthetically simple analogue, **Cy3-GUL**, where a five-atom linker connects the GUL pharmacophore to the cyanine. This is a far closer connection than employed in either of the radiolabels but maintains the steric bulk at approximately the same distance from the GUL pharmacophore as **F-GUL**'s naphthylalanine.
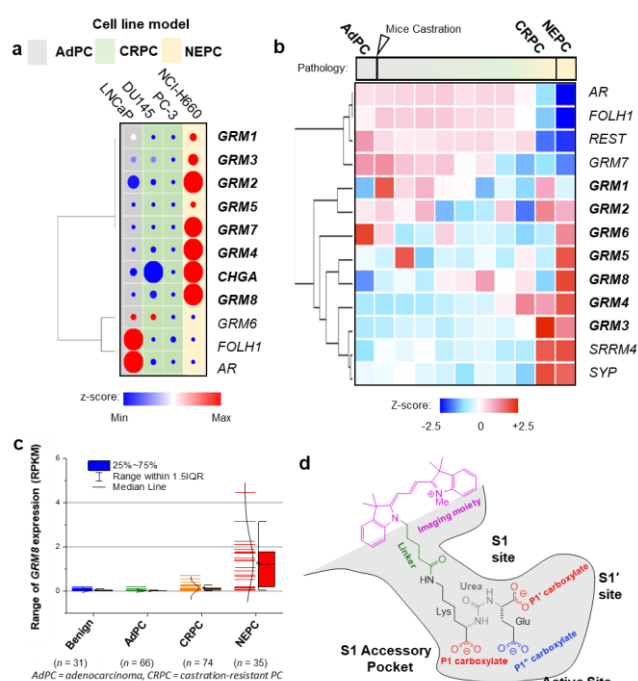

Fig. 3. Differential expression of GRM genes is associated with higher expression of NEPC-markers and shorter times to biochemical relapse. **(a)** The heatmap plot of the expression levels of GRMs levels in well-established AdPC cell lines defined as hormone-sensitive adenocarcinoma prostate cancer (grey), castration-resistant prostate cancer (green) and NEPC (yellow) **(b)** Transcription changes in the GRM genes during progression from AdPC to NEPC in a series of PDX mice models. **(c)** mGluR8 gene expression level in different cohorts of PC. **(d)** Structure of novel probe **Cy3-GUL.**

Comparing the predicted binding of **Cy3-GUL** with PSMA to that of **Ga-GUL** and **F-GUL** suggests that **Cy3-GUL** will adopt a similar pose to **F-GUL**, interacting with one of the Zn^{2+} ions through the P1″ carboxylate (**Fig. 4a**). **Cy3-GUL** forms fewer and less consistent hydrogen bonding interactions than the other probes and, unlike **Ga-GUL**, but like **F-GUL,** it does not enter the S1′ pocket; it also lacks **F-GUL**'s highly charged imaging moiety preventing

a series of cation-π interactions (**Fig. S2c**). However, it does hydrogen bond to Arg534, Ser547, Tyr552 and Tyr700. As a result, greater RMSD fluctuations occur for **Cy3-GUL** during the MD simulation (**Fig. S4**). Although more flexible, **Cy3-GUL** still forms enough key interactions to remain an excellent ligand for PSMA.

Cy3-GUL is predicted to bind very well to NAALADL1 with similar affinity as **F-GUL** and **Ga-GUL** (**Fig. 4c** and **Table 1**). The binding modes of all three probes are different due to the greater size of the NAALADaseL1 active site; however, they all bind with the GUL moiety extended into the binding pocket (**Fig. 4d**). In the case of **Cy3-GUL**, the P1″ carboxylate forms interactions with one of the Zn^{2+} ions (bound to P1 in **Ga-GUL** and P1′ in **F-GUL**). Several strong hydrogen bonds and salt bridges are formed with the receptor (Arg198, Arg539, Tyr544, and Gly195 backbone NH) which stabilize the complex and remain intact throughout the MD simulation. These are similar to those observed for **F-GUL**; however, **F-GUL** forms several additional interactions. Arg198 and Tyr544, are particularly important and form key interactions with all three probes (**Fig. S2f**). **Cy3-GUL** again shows slightly greater fluctuation in the RMSD, largely due to the flexibility in the dye and linker domains due to their less charged nature.

Cy3-GUL shows stronger affinity for mGluR8 than for any of the other mGluRs (**Fig 4e, Table 1, Table S3**), adopting a bound conformation distinct from that of the other two probes (**Fig. 4f**) with the **GUL** moiety buried deep within the highly charged cleft (**Fig. 4e**). Three extremely stable salt bridges are formed between the P1, P1′ and P1″ carboxylates and the Arg255, and Arg188, and Arg255 of the second subunit (**Fig. S2I**). Due to these key interactions, minimal RMSD fluctuations are observed in the RMSD of the MD of the **Cy3-GUL–mGluR8** complex. With both sufficient predicted binding, and close agreement in the binding mode of the GUL pharmacophore to those of the clinical radiolabels, this probe was

synthesized for *in vitro* evaluation, which we accomplished from GUL and our previously prepared cyanine dye (**Fig. S20** and accompanying discussion).[20]

Cy3-GUL binds to PSMA *in vivo*. Flow cytometry demonstrates far stronger uptake of **Cy3-GUL** into PSMA-positive LNCaP cells relative to into PSMA-negative DU145 cells (**Fig. S21a-b**). This indicates that although **Cy3-GUL** is predicted to bind well to three different proteins, it is not generally promiscuous: it requires PSMA to enter the cell (both DU145 and LNCaP have low levels of both mGluRs and NAALADL, **Fig. S21e**). In addition, the PSMA-positive LNCaP do not become fluorescent when they are exposed to the unconjugated dye indicating the GUL moiety is essential for selective uptake (**Fig. S21d**). Similarly, PSMA-negative DU145 cells, an AdPC cell line, show almost no **Cy3-GUL** uptake (**Fig. S21c-d**). Functionally, **Cy3-GUL** exposure shows no cellular toxicity at any tested dose regardless of cell type (**Fig. S22**). This data, along with the computational modeling, suggests that **Cy3-GUL** is an acceptable fluorescent homologue of the two clinically deployed PET reagents; we consequently used it to validate our hypothesis that GUL-probes bind mGluR8 and NAALADL1.

Cy3-GUL Probes are selectively taken up by mGLuR and NAALADaseL1. To investigate the affinity of GUL for mGluR8, we measured the uptake of **Cy3-GUL** in PSMA-negative DU145 cells both with and without overexpression of mGluR8 (**Fig. 5a-c**). LNCaP-PSMA positive cells were used as a positive control. Immunofluorescence microscopy demonstrates a five-fold increase in **Cy3-GUL** uptake when mGLuR8 was overexpressed (**Fig. 5c**). mGluR8's involvement is further supported by its upregulation when PSMA-negative DU145 cells are driven to develop NE features by epidermal growth factor (EGF) and dibutyryl cAMP (db-cAMP) co-treatment and simultaneous serum starvation as previously described (**Fig. 5d & Fig S23a-b**).[40] After treatment, cells display neuronal /neuroendocrine characteristics

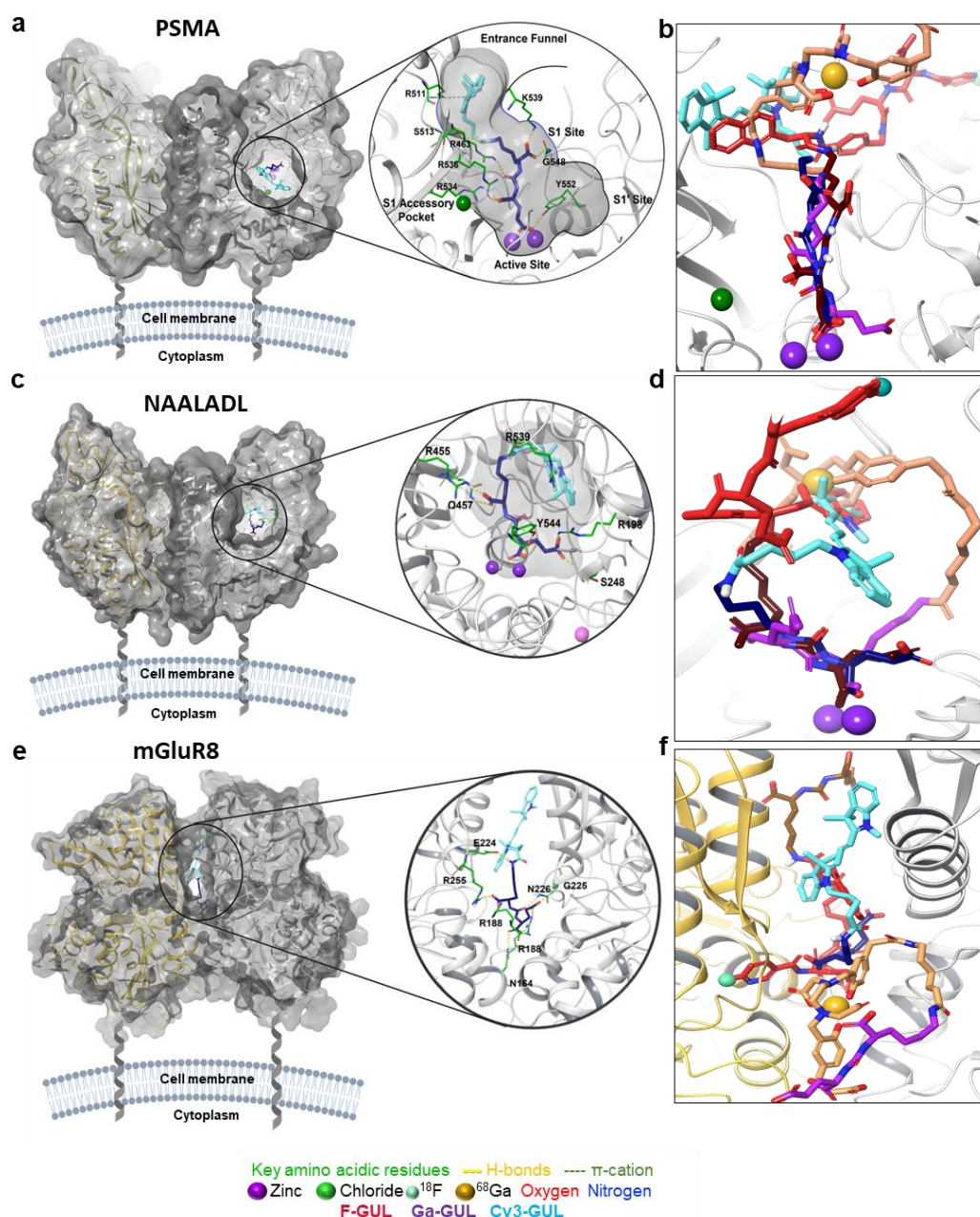including neurite-like outgrowth (Fig. **S23c**), while increasing their expression of select mGluR

Fig. 4. Novel probe Cy3-GUL binds to the PSMA and NAALADL1 active sites and mGluR8 cleft similar to the clinical radiopharmaceuticals. (a) Cy3-GUL's computed conformation within the PSMA active site (*2XEG*). **(b)** Comparison of **Cy3-GUL** (GUL moiety in deep blue, dye in cyan); **Ga-GUL** (GUL moiety in maroon, ligand in red); and **F-GUL** (GUL moiety in purple, pseudopeptide in peach) within the PSMA active site; **(c)** Cy3-GUL's computed conformation within the NAALADL1 active site (*4TWE*). **(d)** Comparison of **Cy3-GUL, Ga-GUL,** and **F-GUL** in the NAALADL1 active site, colouring the same as in (b). **(e)** Cy3-GUL's computed conformation within the mGluR8 cleft (*6BSZ*). **(f)** Comparison of **Cy3-GUL, Ga-GUL,** and **F-GUL** in the mGluR8 cleft, colouring the same as in (b).
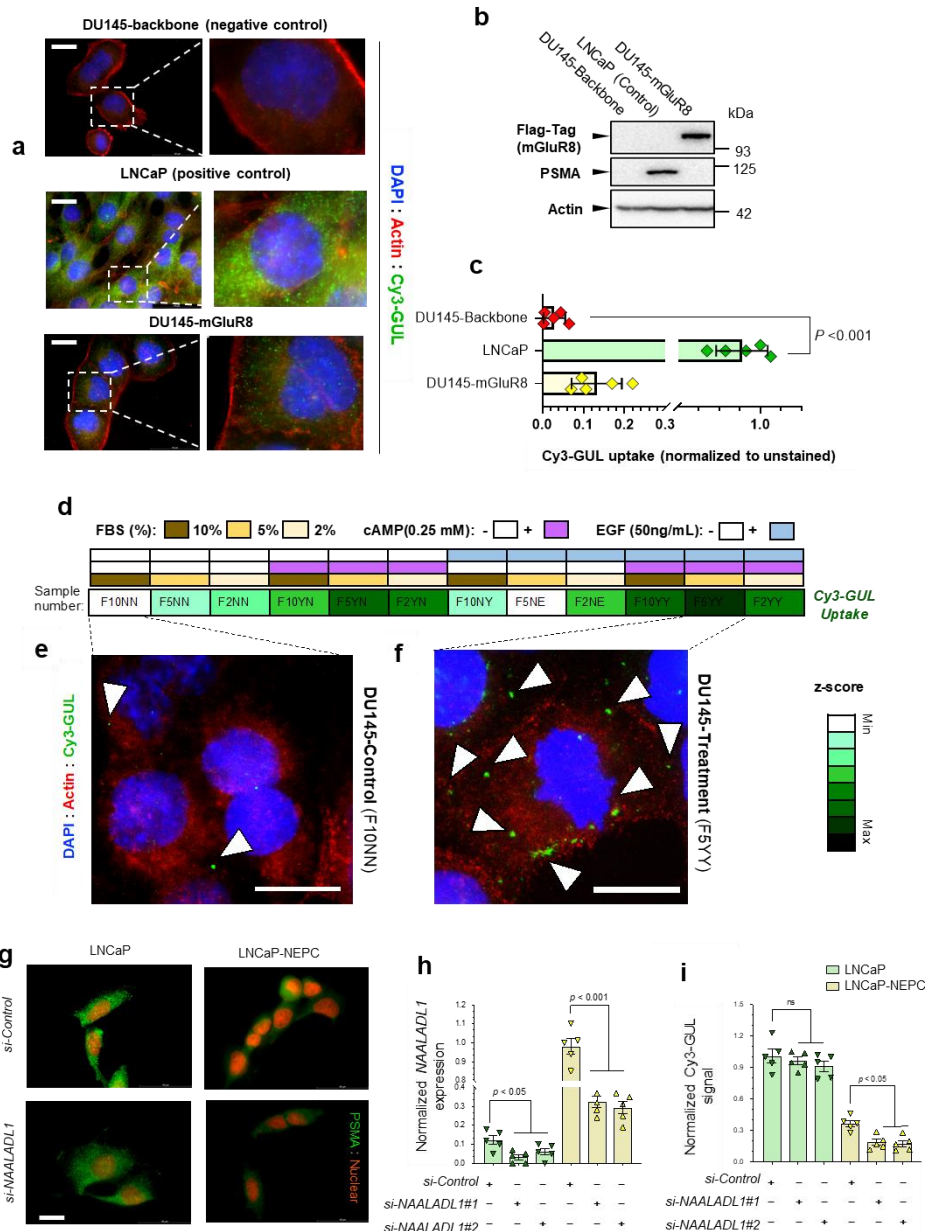
14

Fig. 5 NAALADaseL and MGluR8 regulate update of Cy3-GUL. The overexpression of mGLuR8 in a PSMA-negative cell line induces uptake of **Cy3-GUL**. (**a**) Representative immunocytochemistry images of cells stained with Hoechst (blue), **Cy3-GUL** (green) and actin (red). (**b**) Western blot analyses of PSMA and mGluR8 protein levels; (**c**) Quantification of **Cy3-GUL** uptake, analyzed by one-way ANOVA; (**d**) NE-transdifferentiation of DU145 cell line by EGF/cAMP treatment and serum starvation increases **Cy3-GUL** uptake. DU145 cell line treated with cAMP (0.25 mM), and EGF (50 ng/mL) and gradient levels of FBS while the control group (F10NN model) was treated with 10% FBS. Then after 3 days, the cells were incubated with 100 nM Cy3-GUL for 1 hour and analyzed by PCR and immunocytochemistry; (**e-f**) Representative immunocytochemistry images of cells stained with Hoechst (blue), **Cy3-GUL** (green) and actin (red). The *NAALADL1* gene is upregulated in NEPC cell line model and its inhibition could suppress GUL-ligand uptake; (**g**) Representative images of **Cy3-GUL** uptake in AdPC and NEPC models of LNCaP cell lines following inhibition of *NAALADL1* gene using siRNA technology. Scale bar = 20 microns; (**h**) Quantification of *NAALADL1* gene expression using real time PCR; (**i**) Quantification of **Cy3-GUL** uptake following inhibition of *NAALADL1* gene by flow cytometry.

genes (including *GRM4 and 8*) (Fig. **S23c**). Similarly, differential expression of GRMs was

observed following overexpression of SRRM4 as a regulator of NEPC (**Fig. S24**). Although not expressing PSMA, these cells still significantly increase their uptake of **Cy3-GUL** (**Fig. 5d-f**), supporting our contentions that GUL radiolabels may bind mGluRs such as mGLuR8, and that these mGluRs could be markers of NEPC emergence.

To determine whether NAALADaseL1 can bind **Cy3-GUL**, we performed a knockdown of *NAALADL1* in wild-type LNCaP cells and LNCaP cells driven to a neuroendocrine phenotype (LNCaP-NE) after treatment with charcoal-stripped serum as previously described[17](**Fig. S25** and **Fig 5g-i**). PCR analysis both confirmed the successful *NAALADL1* knockdown and demonstrated that *NAALADL1* gene expression is significantly higher in the LNCaP-NE line over control (**Fig. 5h**). When treated with the probe, **Cy3**-**GUL** uptake positively correlated with NAALADaseL1 levels. **Cy3-GUL** uptake was significantly reduced in LNCaP-NE cells with *NAALADL1* knockdown; however, probe uptake was unchanged in wildtype LNCaP cells despite successful knockdown (**Fig. 5i**). This is likely due to high PSMA expression in LNCaP control cells which was unaffected by *NAALADL1* knockdown (**Fig. 5g,i**).

Conclusion: As cells develop neuroendocrine features, both the *GRMs* and *NAALADL* are upregulated while PSMA-levels fall. The computational data suggests that the GUL probes can bind to these proteins, and they may be responsible for GUL probes' recognition of PSMA-negative metastatic NEPC lesions. Fluorescent analogue **Cy3-GUL** binds to these proteins, validating them as off-target binding targets of GUL. This project highlights the benefits of integrating computational and synthetic chemistry, with data-mining clinical databases and conducting *in vitro* and *in vivo* experiments to accelerate the validation of protein targets. This work explains why caution must be taken on clinical conclusions made with PSMA-targeted imaging alone and suggests that mGLuR and NAALADaseL1 may represent new targets for

imaging and therapeutic purposes. These proteins may play a role in NEPC, and their biochemical importance to this cancer deserves greater attention.

Methods: The materials and methods are described in the Supporting Information. Institutional Review Board and Animal Care Committee of the University of British Columbia approved this study and all subjects signed a written informed consent. All synthetic, computational, molecular biological, and animal model data is available in the SI.

Data and material availability: Data associated with the reported findings are available in the manuscript or supplementary information. Samples of the fluorescent **Cy3-GUL** probe are available on request while current supplies last (contact JFT), although full synthetic details accompany this article allowing for its preparation.

References

1.   Abida W, Cyrta J, Heller G, Prandi D, Armenia J, Coleman I, *et al.* Genomic correlates of clinical outcome in advanced prostate cancer. *Proc Natl Acad Sci U S A* 2019, **116**(23)**:** 11428-11436.

2.   Siegel RL, Miller KD, Jemal A. Cancer statistics, 2020. *Ca-Cancer J Clin* 2020, **70**(1)**:** 7-30.

3.   Siva S, Udovicich C, Tran B, Zargar H, Murphy DG, Hofman MS. Expanding the role of small-molecule PSMA ligands beyond PET staging of prostate cancer. *Nat Rev Urol* 2020.

4.   Zippel C, Ronski SC, Bohnet-Joschko S, Giesel FL, Kopka K. Current Status of PSMA-Radiotracers for Prostate Cancer: Data Analysis of Prospective Trials Listed on ClinicalTrials.gov. *Pharmaceuticals* 2020, **13**(1)**:** 12.

5.   Lesniak WG, Boinapally S, Banerjee SR, Behnam Azad B, Foss CA, Shen C, *et al.* Evaluation of PSMA-targeted PAMAM dendrimer nanoparticles in a murine model of prostate cancer. *Mol Pharm* 2019, **16**(6)**:** 2590-2604.

6.   Baranski AC, Schafer M, Bauder-Wust U, Roscher M, Schmidt J, Stenau E, *et al.* PSMA-11-derived dual-labeled PSMA inhibitors for preoperative PET iaging and precise fluorescence-guided surgery of prostate cancer. *J Nucl Med* 2018, **59**(4)**:** 639-645.

7.   Eder M, Schäfer M, Bauder-Wüst U, Hull W-E, Wängler C, Mier W, *et al.* 68Ga-Complex lipophilicity and the targeting property of a Urea-based PSMA inhibitor for PET imaging. *Bioconjugate Chem* 2012, **23**(4)**:** 688-697.

8.   Ganguly T, Dannoon S, Hopkins MR, Murphy S, Cahaya H, Blecha JE, *et al.* A high-affinity [(18)F]-labeled phosphoramidate peptidomimetic PSMA-targeted inhibitor for PET imaging of prostate cancer. *Nucl Med Biol* 2015, **42**(10)**:** 780-787.

9.   Kuten J, Fahoum I, Savin Z, Shamni O, Gitstein G, Hershkovitz D, *et al.* Head- to head comparison of ^{68}Ga-PSMA-11 with ^{18}F-PSMA-1007 PET/CT in staging prostate cancer using histopathology and immunohistochemical analysis as reference-standard. *J Nucl Med* 2019.

10.   Cardinale J, Martin R, Remde Y, Schäfer M, Hienzsch A, Hübner S, *et al.* Procedures for the GMP-compliant production and quality control of [^{18}F]PSMA-1007: A next generation radiofluorinated tracer for the detection of prostate cancer. *Pharmaceuticals (Basel)* 2017, **10**(4)**:** 77.

11.   Barinka C, Novakova Z, Hin N, Bim D, Ferraris DV, Duvall B, *et al.* Structural and computational basis for potent inhibition of glutamate carboxypeptidase II by carbamate-based inhibitors. *Bioorg Med Chem* 2019, **27**(2)**:** 255-264.

12. Vornov JJ, Peters D, Nedelcovych M, Hollinger K, Rais R, Slusher BS. Looking for drugs in all the wrong places: Use of GCPII inhibitors outside the brain. *Neurochem Res* 2019.

13. Maurer T, Eiber M, Schwaiger M, Gschwend JE. Current use of PSMA–PET in prostate cancer management. *Nat Rev Urol* 2016, **13**(4)**:** 226-235.

14. Kaittanis C, Andreou C, Hieronymus H, Mao N, Foss CA, Eiber M*, et al.* Prostate-specific membrane antigen cleavage of vitamin B9 stimulates oncogenic signaling through metabotropic glutamate receptors. *J Exp Med* 2017, **215**(1)**:** 159-175.

15. Bakht MK, Oh SW, Youn H, Cheon GJ, Kwak C, Kang KW. Influence of androgen deprivation therapy on the uptake of PSMA-targeted agents: Emerging opportunities and challenges. *Nuc Med Molec Imag* 2017, **51**(3)**:** 202-211.

16. Hupe MC, Philippi C, Roth D, Kümpers C, Ribbat-Idel J, Becker F*, et al.* Expression of prostate-specific membrane antigen (PSMA) on biopsies is an independent risk stratifier of prostate cancer patients at time of initial diagnosis. *Front Oncol* 2018, **8:** 623.

17. Bakht MK, Derecichei I, Li Y, Ferraiuolo RM, Dunning M, Oh SW*, et al.* Neuroendocrine differentiation of prostate cancer leads to PSMA suppression. *Endocr Relat Cancer* 2019, **26**(2)**:** 131-146.

18. Beltran H, Prandi D, Mosquera JM, Benelli M, Puca L, Cyrta J*, et al.* Divergent clonal evolution of castration-resistant neuroendocrine prostate cancer. *Nat Med* 2016, **22**(3)**:** 298-305.

19. Bluemn EG, Coleman IM, Lucas JM, Coleman RT, Hernandez-Lopez S, Tharakan R*, et al.* Androgen receptor pathway-independent prostate cancer is sustained through FGF signaling. *Cancer Cell* 2017, **32**(4)**:** 474–489.

20. Bakht MK, Lovnicki JM, Tubman J, Stringer KF, Chiaramonte J, Reynolds MR*, et al.* Differential expression of glucose transporters and hexokinases in prostate cancer with a neuroendocrine gene signature: a mechanistic perspective for FDG imaging of PSMA-suppressed tumors. *J Nuc Med* 2020, **61**(6)**:** 904-910.

21. Spratt DE, Gavane S, Tarlinton L, Fareedy SB, Doran MG, Zelefsky MJ*, et al.* Utility of FDG-PET in clinical neuroendocrine prostate cancer. *Prostate* 2014, **74**(11)**:** 1153–1159.

22. Thang SP, Violet J, Sandhu S, Iravani A, Akhurst T, Kong G*, et al.* Poor outcomes for patients with metastatic castration-resistant prostate cancer with low prostate-specific membrane antigen (PSMA) expression deemed ineligible for 177Lu-labelled PSMA radioligand therapy. *Eur Urol Oncol* 2018, **in press**.

23. Derlin T, Werner RA, Lafos M, Henkenberens C, von Klot CAJ, Sommerlath Sohns J*, et al.* Neuroendocrine differentiation and response to PSMA-targeted radioligand therapy in advanced metastatic castration-resistant prostate cancer: A single-center retrospective study. *J Nucl Med* 2020.

24.   Paschalis A, Sheehan B, Riisnaes R, Rodrigues DN, Gurel B, Bertan C, *et al.* Prostate-specific membrane antigen heterogeneity and DNA repair defects in prostate cancer. *Eur Urol* 2019, **76**(4)**:** 469-478.

25.   Current K, Meyer C, Magyar CE, Mona CE, Almajano J, Slavik R, *et al.* Investigating PSMA-targeted radioligand therapy efficacy as a function of cellular PSMA levels and intra-tumoral PSMA heterogeneity. *Clin Cancer Res* 2020.

26.   Fendler WP, Calais J, Eiber M, Simko JP, Kurhanewicz J, Santos RD, *et al.* False positive PSMA PET for tumor remnants in the irradiated prostate and other interpretation pitfalls in a prospective multi-center trial. *Eur J Nucl Med Mol Imaging* 2020.

27.   Youn S, Kim KI, Ptacek J, Ok K, Novakova Z, Kim Y, *et al.* Carborane-containing urea-based inhibitors of glutamate carboxypeptidase II: Synthesis and structural characterization. *Bioorg Med Chem Lett* 2015, **25**(22)**:** 5232-5236.

28.   Pavlicek J, Ptacek J, Barinka C. Glutamate carboxypeptidase II: An overview of structural studies and their importance for structure-based drug design and deciphering the reaction mechanism of the enzyme. *Curr Med Chem* 2012, **19**(9)**:** 1300-1309.

29.   Machulkin AE, Ivanenkov YA, Aladinskaya AV, Veselov MS, Aladinskiy VA, Beloglazkina EK, *et al.* Small-molecule PSMA ligands. Current state, SAR and perspectives. *J Drug Target* 2016, **24**(8)**:** 679-693.

30.   Barinka C, Byun Y, Dusich CL, Banerjee SR, Chen Y, Castanares M, *et al.* Interactions between human glutamate carboxypeptidase II and urea-based inhibitors: Structural characterization. *J Med Chem* 2008, **51**(24)**:** 7737-7743.

31.   Mesters JR, Barinka C, Li W, Tsukamoto T, Majer P, Slusher BS, *et al.* Structure of glutamate carboxypeptidase II, a drug target in neuronal damage and prostate cancer. *EMBO Journal* 2006, **25**(6)**:** 1375-1384.

32.   Zhang AX, Murelli RP, Barinka C, Michel J, Cocleaza A, Jorgensen WL, *et al.* A Remote Arene-Binding Site on Prostate Specific Membrane Antigen Revealed by Antibody-Recruiting Small Molecules. *J Am Chem Soc* 2010, **132**(36)**:** 12711-12716.

33.   Wu LY, Anderson MO, Toriyabe Y, Maung J, Campbell TY, Tajon C, *et al.* The molecular pruning of a phosphoramidate peptidomimetic inhibitor of prostate-specific membrane antigen. *Bioorg Med Chem* 2007, **15**(23)**:** 7434-7443.

34.   Novakova Z, Wozniak K, Jancarik A, Rais R, Wu Y, Pavlicek J, *et al.* Unprecedented binding mode of hydroxamate-based inhibitors of glutamate carboxypeptidase II: Structural characterization and biological activity. *J Med Chem* 2016, **59**(10)**:** 4539-4550.

35.   Cardinale J, Roscher M, Schaefer M, Geerlings M, Benešová M, Bauder-Wüst U, *et al.* Development of PSMA-1007 - related series of 18F-labeled Glu-ureido type PSMA inhibitors. *J Med Chem* 2020**:** ASAP article.

36.   Pangalos MN, Neefs J-M, Somers M, Verhasselt P, Bekkers M, van der Helm L*, et al.* Isolation and expression of novel human glutamate carboxypeptidases with N-Acetylated α-linked acidic dipeptidase and dipeptidyl peptidase IV activity. *J Biol Chem* 1999, **274**(13)**:** 8470-8483.

37.   Sippl MJ, Wiederstein M. Detection of spatial correlations in protein structures and molecular complexes. *Structure* 2012, **20**(4)**:** 718-728.

38.   Akamatsu S, Wyatt AW, Lin D, Lysakowski S, Zhang F, Kim S*, et al.* The placental gene PEG10 promotes progression of neuroendocrine prostate cancer. *Cell Rep* 2015, **12**(6)**:** 922-936.

39.   Taylor BS, Schultz N, Hieronymus H, Gopalan A, Xiao Y, Carver BS*, et al.* Integrative genomic profiling of human prostate cancer. *Cancer Cell* 2010, **18**(1)**:** 11-22.

40.   Humez S, Monet M, Legrand G, Lepage G, Delcourt P, Prevarskaya N. Epidermal growth factor-induced neuroendocrine differentiation and apoptotic resistance of androgen-independent human prostate cancer cells. *Endocr Relat Cancer* 2006, **13**(1)**:** 181-195.

Supplemental Videos captions

Suppl. Video 1 The 3D computational modeling of **Cy3-GUL** with active site of PSMA.

Suppl. Video 2 The 3D computational model of **Cy3-GUL** with the active site of NAALADaseL.

Suppl. Video 3 The 3D computational model of **Cy3-GUL** with the mGluR8 homodimer.

Suppl. Video 4 The 3D computational modeling of **F-GUL** with active site of PSMA.

Suppl. Video 5 The 3D computational model of **F-GUL** with the active site of NAALADaseL.

Suppl. Video 6 The 3D computational model of **F-GUL** with the mGluR8 homodimer.

Suppl. Video 7 The 3D computational modeling of **Ga-GUL** with active site of PSMA.

Suppl. Video 8 The 3D computational model of **Ga-GUL** with the active site of NAALADaseL.

Suppl. Video 9 The 3D computational model of **Ga-GUL** with the mGluR8 homodimer.